Spectral Characteristics of Antimony-Phosphate Glass

[1]Soham Younis, [2*]M. R. Sahar and [3]S.K. Ghoshal

[1, 2, 3]Advanced Optical Materials Research Group, Department of Physics, Faculty of Science, Universiti Teknologi Malaysia, 81310 UTM Johor Bahru, Johor, Malaysia

[1]Seham_yns@yahoo.com, [2*]rahimsahar@utm.my, [3]sibkrishna@utm.my
*Corresponding author

Abstract. Determining the stable optimized compositions of the binary and ternary phases of antimony-phosphate glasses is the key issue. We prepare four series of glasses of the form (100-x)Sb_2O_3-xP_2O_5, where x = 30, 40, 50, 60 and 70 mol%, (95-x)Sb_2O_3-xP_2O_5-5MgO, where x = 60, 45, 40, 35, 30 and 25 mol%, (85-x)Sb_2O_3-xP_2O_5-15MgO, where x = 60, 45, 40, 35, 30 and 25 mol% and (75-x)Sb_2O_3-xP_2O_5-25MgO, where x = 60, 45, 40, 35, 30 and 25 mol% via conventional melt quenching method. Structural and optical properties of these glasses are determined through FTIR, UV-Vis and PL measurements. The XRD patterns confirm the amorphous nature of samples. The FTIR spectra of all prepared glass series recorded in the spectral ranges of 400 to 4000 cm^{-1} demonstrates the presence of asymmetric stretching vibrations of $(PO3)^2$, Sb_2O_3 doubly degenerate stretching vibrations, stretching vibration of P–O–Sb linkages, vibration modes of SbO_3 of the valentinite and vibration modes of SbO_3 of the valentinite. The UV-Vis absorption spectra in the wavelength range of 200-2000 nm exhibit a broad transparency range with short wavelength absorption edge located at around 380 nm. A small shift of the absorption edge due to the change in glass composition is evidenced. The room temperature emission spectra under four different excitation wavelengths such as 300, 380, 550 and 780 nm display single sharp second harmonic emission peak at half wavelength and double frequency of the excitation wavelength. Glasses reveal low durability against humidity at higher P_2O_5 concentration exceeding 65 mol%. Furthermore, initiation of glass formation begins when Sb_2O_3 concentration is found to be less than or equal to 40 mol% for the binary system and 60 mol% for the ternary one. These promising features of the optical properties are highly useful for widespread photonic applications.

Keywords Melt-quenching, Antimony-Phosphate glass, optical band gap, vibrational spectra

1.0 INTRODUCTION

Glass being the integrated part of human civilization can be engineered with excellent homogeneity in a variety of forms and sizes starting from small fibres to meter-sized pieces. Furthermore, they can be doped with rare-earth ions and microcrystallites to obtain a wide range of properties suitable for various applications. These advantages of glass over crystalline materials are due to their unique structural and thermodynamic features [1, 2]. Lately, the focus is shifted towards the development of specialized or exotic glasses as a novel media for photonic, plasmonic and nanophotonic technologies. To achieve these target luminescent rare-earth ions, metal nanoparticles (NPs), semiconductor NPs and their hybrids are incorporated into the glass [1, 3, 4]. The rapid research expansion led to emerging areas with new glass compositions. Unlike traditional silicate, borate and phosphate glasses the heavy metal oxide glasses such as bismuth, tellurite, lead, and/or antimony are emerged as novel glass structure network formers. They played an active role with numerous exciting properties including high refractive index, large transmission window, large non-linear optical properties, low phonon energy (resonance vibration of the matrix) and high dielectric constant. Although, considerable attention is paid on Bi-, Te- and Pb- glasses but Sb-based glasses are

not widely explored [5]. Nonlinear optical (NLO) properties are observed by photoluminescence spectroscopy. The unusual electronic polarization of material is related to electro-optical effect, conductivity and refractivity [6].

Antimony is promising for photonic applications [7] due to their distinctive properties such as transmittance window from 380 to 2000 nm, linear refractive index of ≈ 2 glass transition temperature of 300 °C and high thermal stability [8, 9]. Many efforts are dedicated to synthesize pure antimony glass without much success [10]. For Sb_2O_3 more than 50 mol% the weak field strength of Sb^{3+} cation (0.73), high volatilization rate and preferred crystallization inhibit their formation [11, 12]. In the glass network SbO_3 structural units occur in the form of trigonal pyramids where the oxygen atoms occupy three corners and a lone pair of electrons of antimony at the fourth corner. In fact, the presence of this pair enhances the nonlinear optical susceptibility in the antimonite glasses described by third rank polar tensors [13]. Antimony may also exist in fifth oxidation state, participating in the formation of glass network with SbO_4 structural units. Recently, the effect of increasing Sb_2O_3 contents on various properties of zinc borophosphate glasses is reported [14]. The influence of increasing Sb_2O_3 contents on thermal, chemical and physical properties of pure V_2O_5-P_2O_5 glass are reported [15]. Bing Zhang examined the impact of Sb_2O_3 on the network structure, thermal stability and chemical durability of $ZnO–P_2O_5$ glasses [16]. Sudarsan studied the structure and optical behaviours of PbO-P_2O_5-Sb_2O_3 [17].

In this view, new ternary antimonite glass systems of the form Sb_2O_3-P_2O_5-MgO are prepared. To the best of our knowledge, we scrutinize for the first time the glass formation range, physical, optical and structural properties of such glasses via in-depth analyses.

2.0 MATERIAL AND METHODS

Four series of ternary glasses with the compositions (in mol%) of (100-X)Sb_2O_3-XP_2O_5, where X = 30, 40, 50, 60 and 70, (95-X) Sb_2O_3-X P_2O_5-5MgO (X=35, 40, 45), (85-X) Sb_2O_3-X P_2O_5-15Mg (X= 25, 35, 55) and (75-X) Sb_2O_3-X P_2O_5-25MgO (X= 25, 35, 45), were synthesized from high purity analytical grade oxides of Sb_2O_3, P_2O_5, and MgO via conventional melt quenching technique. About 7 gm of constituent materials was thoroughly mixed and pre-treated at 300 °C for 1 h to reduce the bubbles in the glass and to avoid the volatility of P_2O_5 at high temperature. The mixture was then melted in a muffle furnace at 1050 °C for 1 h. After achieving the required viscosity the melt was quenched into a preheated steel plate at 300 °C to form disc-shaped samples before being annealed at 300 °C for 2 h to release stress. Then, the furnace was switched off and the sample was cooled down to room temperature. Samples were finally cut and polished to a dimension of 2 mm x 4 mm for further characterizations at room temperature.

The amorphous nature of the prepared samples is determined via X-ray diffraction (XRD) where a Siemens X-ray Diffractometer D5000 equipped with diffraction software analysis is used. It used CuKα radiation and operated at 40 kV, 30 mA. The diffraction peaks are measured in the 2Θ range of 10 to 80°, in the step of 0.05 and 1s counting time per step. Glass density (ρ) was measured by using Archimedes' method with toluene as immersion liquid. Physical properties such as molar volume (V_m), oxygen packing density, ion concentration and total packing fraction were calculated. To determine the vibrational modes, Fourier transmission infrared (FTIR) measurement was performed using a Perkin-Elmer 1710 Fourier transformed infrared spectrometer over the range of 4000-400 cm^{-1}. UV-VIS spectra were recorded using Perkin-Elmer UV-VIS-NIR Lamda 900 spectrometer. A Deuterium lamp (DL) and halogen lamp (HL) were used as a radiation sources. Direct and indirect optical band gaps are calculated from Mott and Davis equation [18]:

$$\alpha\ (\omega) = B\ \frac{(\hbar\ \omega - E_{opt})^{n}}{\hbar\ \omega} \quad (1)$$

where α is the frequency (ω) dependent absorption, B is a constant and E_{opt} is the band gap energy for direct (n=1/2) and indirect (n=2) transitions. The refractive index n was calculated using Dimitrov and Sakka formula [19]. The molar refraction (R_m) and the electronic polarizability(α_m) of the glass samples were calculated using Lorentz - Lorenz equation.

The Urbach energy (ΔE) or band tail signifying the disordered amorphous nature of materials was calculated ln α(ω) versus photon energy (hω) plot via [20].

$$\alpha\ (\omega) = A\ exp\left(\frac{\hbar\ \omega}{\Delta E}\right) \quad (2)$$

3.0 RESULTS AND DISCUSSION

Table 3.1 to Table 3.4 summarizes the nominal compositions of all prepared galsses with their physical properties. Figure 3.1 indicates three types of transparent glass samples including ceramic (Opaque) and glass with low chemical durability, hereinafter referred as blue, black and red, respectively. The increase in Sb_2O_3 or MgO concentration enhances the resistance against humidity. The lone pair electron of the antimony oxide interacts with water molecules and act as shield. Further addition of MgO as network modifier increase the rupture of the bridging oxygen bonds and thereby protect the network structure from moisture attack [16].

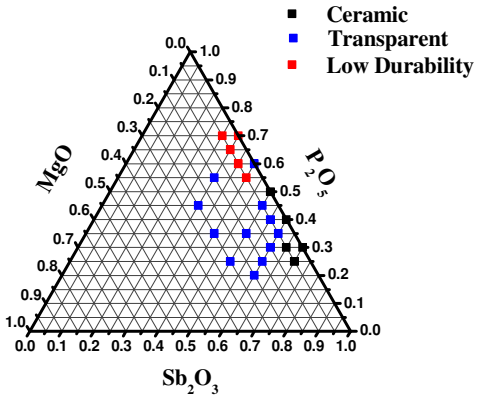

Figure 3.1: Glass Formation Region.

Fig 3.2 clearly displays the increase of glass density and molar volume with the increase of both Sb_2O_3 and MgO. This increase in density with increasing MgO concentration is ascribed to the breakage of bridging oxygens (BOs) bonds and subsequent creation of non-bridging oxygens (NBOs) in the glass network. The increase in glass compactness is related to the occurrence of higher atomic radius of Sb^{3+} (0.9 Å) and magnesium (0.86 Å) compared to phosphorus (0.3 Å) [21].

Table 3.1 The composition and physical properties of (80-X) Sb_2O_3-X P_2O_5 (X=10, 20, 30, 40) glass.

Concentration of Sb_2O_3 (mol%)	ρ (gm/cm^3)	M_w (gm/mole)	V_m (cm^3/mole)	Sb Ion packing density (ion/cm3) × 10^{21}	P Ion packing density (ion/cm3) × 10^{21}	Mg Ion packing density (ion/cm3) × 10^{21}	Oxygen Packing Density (g-atom/liter)	packing Fraction (pf) ×10^{-25}
40	3.75	201.77	53.71	8.97	13.44	0	78.19	1.429

Table 3.2 The composition and physical properties of (95-X) Sb_2O_3-X P_2O_5-5MgO (X=35, 40 ,45) glass.

Concentration of Sb_2O_3 (mol%)	ρ (gm/cm^3)	M_w (gm/mole)	V_m (cm^3/mole)	Sb Ion packing density (ion/cm^3) × 10^{21}	P Ion packing density (ion/cm^3) × 10^{21}	Mg Ion packing density (ion/cm^3) × 10^{21}	Oxygen Packing Density (g-atom/liter)	packing Fractions (pf) ×10^{-25}
50	4.13	211.64	51.23	11.75	10.57	1.17	74.16	1.5
55	4.25	219.12	51.5	12.86	9.35	1.16	71.81	1.49
60	4.37	226.6	51.81	13.94	8.13	1.16	69.47	1.48

Table 3.3 The composition and physical properties of (85-X) Sb_2O_3-X P_2O_5-15MgO (X= 25, 35, 55) glass.

Concentration of Sb_2O_3 (mol%)	ρ (gm/cm^3)	M_w (gm/mole)	V_m (cm^3/mole)	Sb Ion packing density (ion/cm^3) × 10^{21}	P Ion packing density (ion/cm^3) × 10^{21}	Mg Ion packing density (ion/cm^3) × 10^{21}	Oxygen Packing Density (g-atom/liter)	Packing Fraction (pf) ×10^{-25}
30	3.63	171.56	47.23	7.65	14.02	3.82	80.44	1.62
50	4.06	201.48	49.57	12.14	8.5	3.64	68.57	1.54
60	4.48	216.44	48.23	14.98	6.24	3.74	66.34	1.59

Table 3.4 The composition and physical properties of (75-X) Sb_2O_3-X P_2O_5-25MgO (X= 25, 35, 45) glass.

Concentration of Sb_2O_3 (mol%)	ρ (gm/cm^3)	M_w (gm/mole)	V_m (cm^3/mole)	Sb Ion packing density (ion/cm^3) × 10^{21}	P Ion packing density (ion/cm^3) × 10^{21}	Mg Ion Packing density (ion/cm^3) × 10^{21}	Oxygen Packing Density (g-atom/liter)	packing Fraction (pf) ×10^{-25}
30	3.68	161.40	43.77	8.25	12.38	6.87	77.67	1.75
40	4.01	176.36	43.93	10.96	9.59	6.85	72.82	1.74
50	4.31	191.31	44.35	13.57	6.78	6.78	67.63	1.73

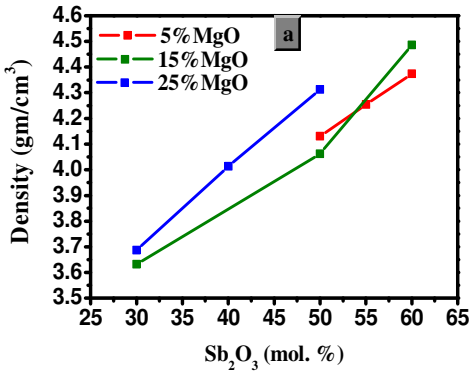

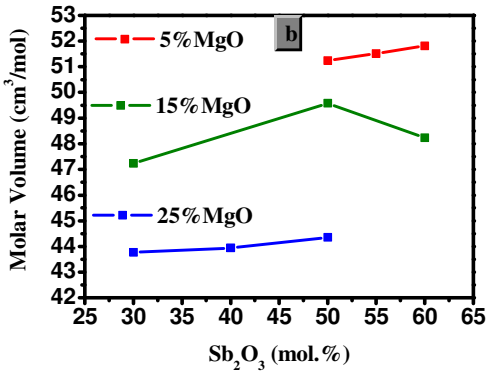

Figure 3.2 (a): Glass density as function of Sb_2O_3 mole percent**. (b):** Glass molar volume as function of Sb_2O_3 mole percent.

The typical XRD pattern (Fig. 3.3) in the presence of a broad hump between 25° and 35° without any sharp peaks clearly confirm the amorphous nature of the prepared glass sample.

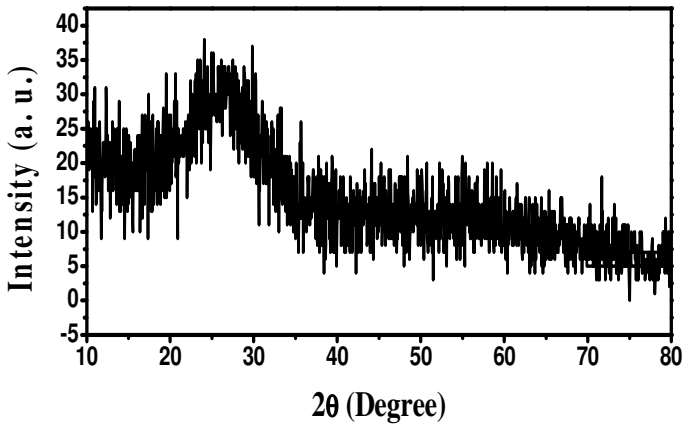

Figure 3.3: XRD pattern of $60Sb_2O_3$-$35P_2O_5$-5MgO glass.

Optical parameters of all the samples in every series are listed in table 3.5 to table 3.7. Fig. 3.4(a)-(c) shows the decrease in E_{opt} with the increase of in Sb_2O_3 concentration irrespective of MgO contents. The addition of MgO leads to the increase of NBOs. Since NBOs are more easily excited than BOs, E_{opt} decreases with addition of MgO and removal of Sb2O3. The variation of optical band gap energy is converse to the Urbach energy. Therefore, the addition of MgO as network modifier would make the glass more loosely packed via the formation of more NBOs and thereby make the glass unstable. The Urbach energy is a measure of random fluctuations of the internal disorder of the glass system which originates from the conversion of weak bonds into defects. In addition, NBOs also affect the glass refractive index, because NBOs possess a higher amount of polarizability compared to BOs. Furthermore, this higher polarizability of Sb^{3+} cation with a lone pair of electrons and high polarization the O^{2-} anion which are responsible for the increase of total electronic polarizability and hence the refractive index [22].

Table 3.5 Direct and indirect band gap energy, Urbach energy (ΔE), refractive index, ,olar refraction and polarizability for glass series (95-X) Sb_2O_3-X P_2O_5-5MgO (X=35, 40 ,45).

Concentration of Sb_2O_3 (mol%)	E_g (Direct) (eV)	E_g (Indirect) (eV)	ΔE_{tail} (eV)	Refractive Index	Molar Refraction Rm (cm^3/mole)	Polarizability α (Å^3/particle)
50	3.69	3.57	0.33	2.23	29.19	11.58
55	3.7	3.55	0.46	2.23	29.34	11.64
60	3.7	3.55	0.48	2.23	29.52	11.71

Table 3.6 Direct and indirect band gap energy, Urbach energy (ΔE), refractive index, ,olar refraction and polarizability for glass series (85-X) Sb_2O_3-X P_2O_5-15MgO (X= 25, 35, 55).

Concentration of Sb_2O_3 (mol%)	E_g (Direct) (eV)	E_g (Indirect) (eV)	ΔE_{tail} (eV)	Refractive Index	Molar Refraction Rm (cm^3/mole)	Polarizability α (Å^3/particle)

30	3.49	3.21	0.57	2.27	27.42	10.88
50	3.37	3.08	0.61	2.3	29.17	11.57
60	3.27	3.02	0.97	2.32	28.63	11.36

Table 3.7 Direct and indirect band gap energy, Urbach energy (ΔE), refractive index, ,olar refraction and polarizability for glass series (75-X) Sb_2O_3-X P_2O_5-25MgO (X= 25, 35, 45).

Concentration of Sb_2O_3 (mol%)	E_g (Direct) (eV)	E_g (Indirect) (eV)	ΔE_{tail} (eV)	Refractive Index	Molar Refraction Rm (cm^3/mole)	Polarizability α (Å^3/particle)
30	3.49	3.22	0.5	2.27	25.41	10.08
40	3.72	3.13	0.45	2.22	24.91	9.88
50	3.23	2.92	0.66	2.33	26.44	10.49

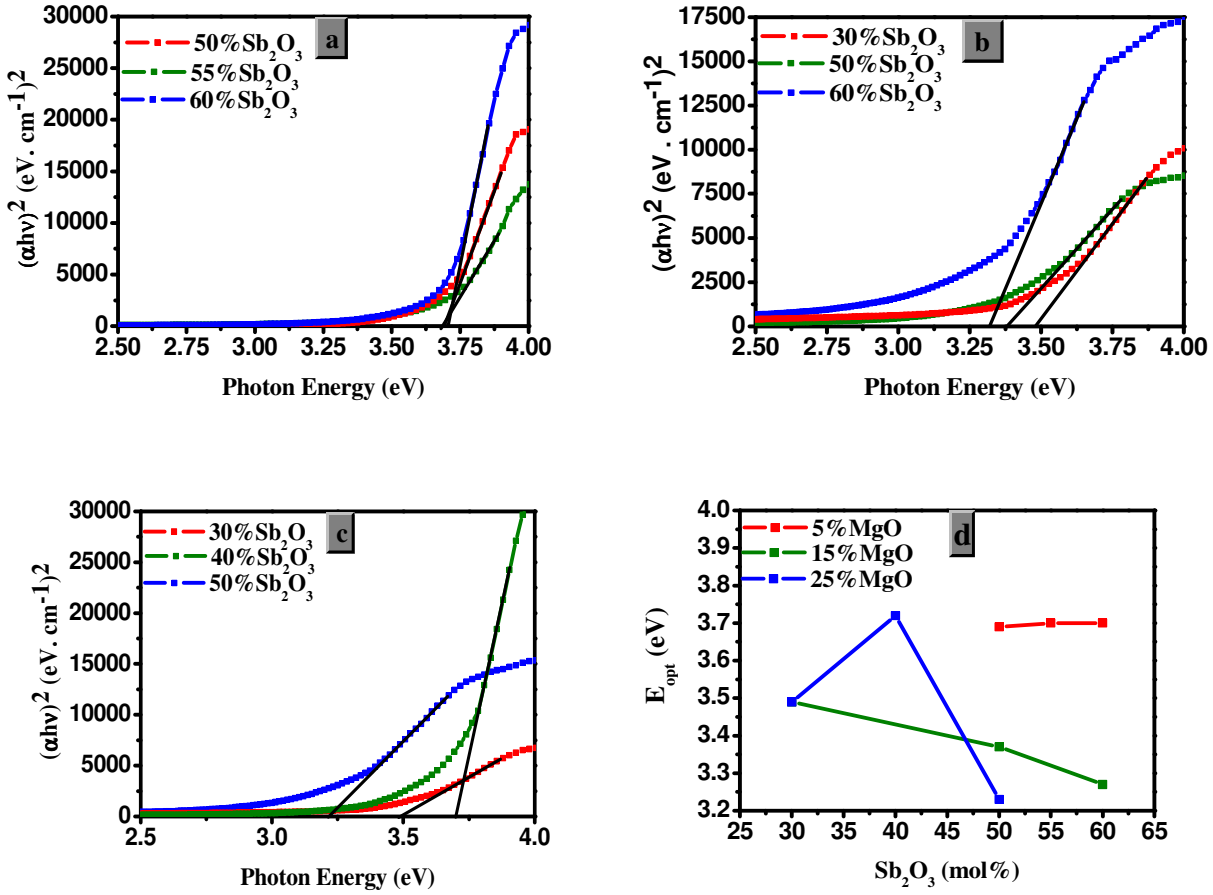

Figure 3.4 Plot of $(\alpha h)^2$ versus (hν) for glass series **(a)** (95-X) Sb_2O_3-X P_2O_5-5%MgO (X=35, 40, 45). **(b)** (85-X) Sb_2O_3-X P_2O_5-15%MgO (X=25, 35, 55), **(c)** (75-X) Sb_2O_3-X P_2O_5-25MgO (X=25, 35, 45) and **(d)** Sb_2O_3 concentration dependent direct band gap energy for three glass series.

Emission spectra of all prepared glasses are recorded in the wavelength range of 200 to 800 nm under four excitation wavelengths of 300, 380, 550 and 780 nm. Fig 3.5 displays the emission spectra of glass series under 780 nm excitations. The appearance of a sharp emission band at 390 nm signifies the light generation at half wavelength and double frequency called second harmonic generation (SHG). This demonstrates the NLO properties of ternary antimonite glass.

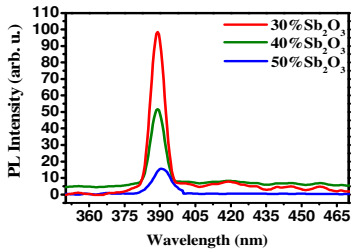

Figure 3.5: The emission spectra of glass series (75-X) Sb_2O_3-X P_2O_5-25MgO (X= 25, 35, 45)

The FTIR spectra (Fig 3.6) of the same glass series is recorded (spectral range of 400 cm^{-1} to 4000 cm^{-1}) to obtain the structural information in terms of bonding vibrations. The corresponding peaks assignments are listed in table 3.8. The spectra comprising of three vibrational modes of SbO_3 of the valentinite in the form of Sb_2O_3 ν3, ν4 and Sb_2O_3 doubly degenerate stretching vibrations ν3 confirm valentinite phase of the glass [22]. In addition, the appearance of stretching vibration of P–O–Sb linkages verifies the participation of PO_4 tetrahedra (Orthophosphate tetrahedra) in the network structure [16]. The occurrence of symmetric and antisymmetric vibration of (PO_2) and vibrations of the O–P–O bonds of Q^1 and Q^2 tetrahedra with non-bridging oxygens (NBOs) confirm the breaking of phosphate network structure. The phosphate structure consists of chains from Q^2 terminated by Q^1 units [16].

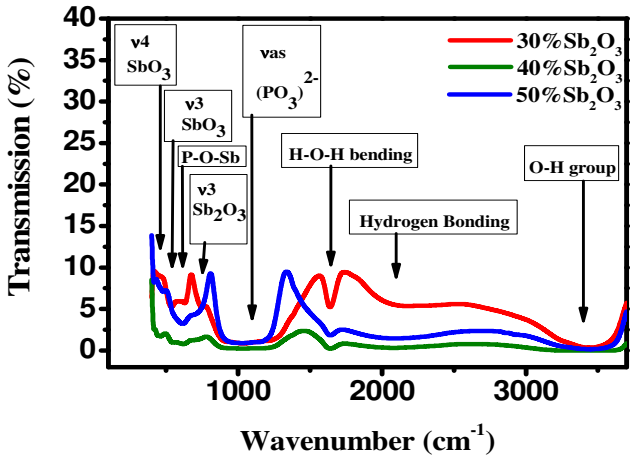

Figure 3.6: FTIR spectra of glass series (75-X) Sb_2O_3-X P_2O_5-25MgO (X= 25, 35, 45)

Table 3.8 FTIR spectral band assignments (in cm^{-1}) of glass series (75-X) Sb_2O_3-X P_2O_5-25MgO (X= 25, 35, 45).

Concentration of Sb_2O_3 (mol%)	Band Assignment							
	v4 vibration modes of SbO3 of the valentinite form of Sb2O3	v3 vibration modes of SbO3 of the valentinite form of Sb2O3	stretching vibration of P–O–Sb linkages	Sb2O3 doubly degenerate stretching vibrations v3	asymmetric stretching vibrations of (PO3)2-	H-O-H bending	Hydrogen bonding	Fundamental stretching of O-H group
30	444	536	629	750	1034	1639	2176	3434
40	461	537	619	711	1036	1639	2081	3392
50	480	530	614	717	1040	1641	2080	3432

3.0 CONCLUSIONS

Four series of new ternary Sb_2O_3-P_2O_5-MgO glasses are synthesized via melt quenching method. Their spectral features are examined as a function of MgO concentration. The FTIR spectra revealed the presence of various stretching vibrational modes of SbO_3 of the valentinite structures. A broad transparency range with short wavelength absorption edge is evidenced from UV-Vis measurements. Emission spectra exhibited single sharp second harmonic peak at half wavelength and double frequency of the excitation wavelength. At higher P_2O_5 concentration the chemical durability of glass is reduced. The physical and optical properties showed considerable improvements.The glass formation began for Sb_2O_3 concentration less than or equal to 40 mol% for the binary system and 60 mol% for the ternary one. The composition is optimized. The influence of MgO on spectral, structural and physical properties are analyzed and understood.

ACKNOWLEDGEMENTS

The authors gratefully acknowledge the financial support from UTM and Malaysian Ministry of Education through Vot.05H36 (GUP) and 4F424 (FRGS).

REFERENCES

[1] Masayuki Yamane, Yoshiyuki Asahara, Glasses for Photonics, 2004, Cambridge, United Kingdom
[2] K. Hirao T. Mitsuyu J. Si J. Qium, Active Glass for Photonic Devices Photoinduced Structures and Their Application, 2001, Springer
[3] Gonella, F. and Mazzoldi, P. (2000). "Metal Nanocluster Composite Glasses." In: Handbook of Nanostructured Materials and Nanotechnology. Nalwa H. S., Ed., vol 4, San Diego, Academic Pres,.
[4] Prasad, P. N. (2004). Nanophotonics. New Jersey, Wiley
[5] James E. Shelby, Introduction to Glass Science and Technology, 2ed Second Edition, Royal Society of Chemistry, (2005)
[6] E.M. Vogel, M.J. Weber, D.M. Krol, Phys. Chem. Glass, 1991, 231.
[7] N G Connelly, T Damhus, R M Hartshorn, A T Hutton, Nomenclature of Inorganic Chemistry, IUPAC Recommendations. 2005
[8] Haxel G, Hedrick J, Orris J., Rare earth elements critical resources for high technology, United States Geological Survey. USGS Fact Sheet, (2006)
[9] S. D. Barrett, S. S. Dhesi, The Structure Of Rare-Earth Metal Surface, Imperial College Press, (2001)
[10] Tirtha Som, Basudeb Karmakar, Efficient green and red fluorescence upconversion in erbium doped new low phonon antimony glasses, Optical Materials 31 (2009) 609–618
[11] Aliff Rohaizada, Rosli Hussina, Nur Aimi Syaqilah Aziza, Royston Uninga, Nur Zu Ira Boharia , Vibrational Studies of Zinc Antimony Borophosphate Glasses Doped Rare Earth, Jurnal Teknologi (Sciences and Engineering). 2013; 62(3):119-122.
[12] Werner Vogel, Glass Chemistry, (1994) Springer-Verlag
[13] T. Satyanarayanaa, I.V. Kityk, K. Ozgac, M. Piasecki, P. Bragiel, M.G. Brike, V. Ravi Kumar, A.H. Reshakf, N. Veeraiaha, Role of titanium valence states in optical and electronic features of PbO–Sb2O3–B2O3:TiO2 glass alloys, Journal of Alloys and Compounds 482 (2009) 283–297
[14] L. Koudelka, J. Sˇ ubcˇı´k, P. Mosˇner, L. Montagne, L. Delevoye, Structure and properties of Sb2O3-containing zinc borophosphate glasses, J.Non-Cryst. Solids 353(2007) 1828.
[15] Aswini GHOSH, B.K. CHAUDHURI, Anomalous Conductivity and other Properties of V2O5-P2O5 Glasses With Bi2O3 Or Sb2O3, Journal of Non-Crystalline Solids 103 (1988) 83-92 83
[16] Bing Zhang, Qi Chen, Li Song, Huiping Li, Fengzhen Hou, The Influence of Sb2O3 Addition on the Properties of Low-melting ZnO–P2O5 Glasses, J. Am. Ceram. Soc., 91 [6] 2036–2038 (2008)
[17] V. Sudarsan, S.K. Kulshreshtha, Study of structural aspect of PbO-P2O5-Sb2O3 glasses, Journal of non-crystalline solids 286 (2001) 99 -107
[18] Al-Ani, S.K.J., Hogarth, C.A. and El-mallawany, R.A.H. A study of optical absorption in tellurite and tungsten-tellurite glasses. J. Mater. Sci., 1985, 20:661-667.
[19] Dimitriv, V. and Sakka, S. Electronic oxide polarizability and optical basicity of simple oxides. I. J. Appl. Phys., 1996, 79:1736-5.
[20] Urbach, F. The Long-Wavelength Edge of Photographic Sensitivity and of the Electronic Absorption of Solids. Phys. Rev., 1953, 92:1324-1324.

[21] Hooi Ming Oo, Halimah Mohamed-Kamari, Wan Mohd Daud Wan-Yusoff, Optical Properties of Bismuth Tellurite Based Glass, Int. J. Mol. Sci. 2012, 13, 4623-4631

[22] Tirtha Som, Basudeb Karmakar, Antimony Oxide Glasses and their Nanocomposites for Optical, Photonic and Nanophotonic Applications, Manueh Razeghi Editor, Antimony Characteristics, Compounds and Applications, Nova Science Publishers, Inc. New York, Chapter 7